Ninth International Conference on Computational Fluid Dynamics (ICCFD9), Istanbul, Turkey, July 11-15, 2016

ICCFD9-2016-329

Multiphase modelling of compressible diesel fuel in a solenoid valve injector

Nuray Kayakol

Bosch Sanayi ve Ticaret A.S. Diesel Systems / Engineering Injectors Nozzles
Organize Sanayi Bölgesi, Eflatun Cad.11 16159 Bursa Turkey

nuray.kayakol@tr.bosch.com

Abstract: Two-phase flow characteristics of a ball type solenoid valve for diesel common rail injectors are modelled with a mixture model approach, which is suited for bubble-liquid flow. The predictive accuracy of a cavitation model based on Rayleigh-Plesset equation and cavitation erosion based on work-hardening of material is dependent on non-geometrical model coefficients. Time dependent cavitation efficiency is defined using valve seat throttling limit which is a threshold ball lift for reaching cavitating regime. Microjet velocity calculated from the bubble interface velocity produces pressure impulse which is smaller than the material yield strength. The compressibility of diesel fuel is taken into account but without modification of cavitation model the solution of energy equation with momentum equation does not show thermal effect on cavitation.

Keywords: Cavitation, multiphase, computational fluid dynamics, solenoid valve, bubble dynamics, turbulence.

1 Introduction

Diesel engines are traditionally known for fuel economy and long service life. In the first and second generation of Bosch's Common Rail diesel fuel Systems (CRS), the injection process is controlled by a magnetic solenoid on the injectors [1]. High injection pressure is the requirement of more efficient combustion. Until the mid 1980's diesel fuel injection systems for light vehicles operated at pressure of 300-400 bar [2]. Today, modern CRS applications utilize maximum injection pressure of 2500 bar and above. More information about CRS can be found elsewhere [3].

A typical CRS fuel injector with electromagnetic fuel injection control is shown in Figure 1. A solenoid valve is used for control of fluid mass flow rates in a fuel injection system. In closed position, the rail pressure is present in both the control chamber above the control plunger and the nozzle chamber. Because the area of the top of the control plunger is larger than the area of the needle-shoulder in the nozzle chamber, a net closing force is present. The needle tip is pushed on its seat and no injection of fuel can take place. When the solenoid in the top of the injector is energized, the resulting magnetic force lifts the ball valve from its seat. Because the flow rate through the Z-throttle is smaller than the flow rate through the A-throttle, the pressure in the control chamber drops. The rail pressure is still present in the nozzle chamber and the needle is pushed upwards, starting the injection of fuel. As the current through the solenoid is stopped, the solenoid spring forces the ball valve back on its seat. As a result, the pressure in the control chamber increases again and the needle is pushed down on its seat, thus stopping the injection [4].

Cavitation is observed in many hydrodynamic mechanical devices, such as pumps, turbines, nozzles and marine propellers, and can have an intensive effect on the performance of these devices.

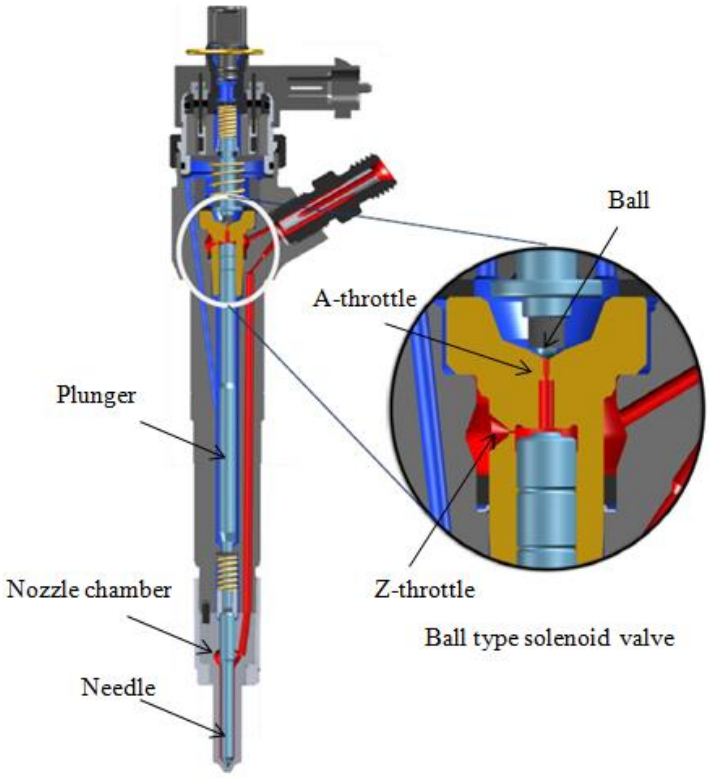

Figure 1. Cross section of Bosch common rail solenoid ball valve injector.

Solenoid valve injector flow shows characteristics of bubbly flow. In the valve seat region of solenoid valves the expansion of fuel flow from high pressure to low pressure regions creates bubbles. Cavitation bubbles originate from cavitation nuclei which are contained in the liquid as gaseous micro bubbles. When local pressure drops below vapour pressure, micro bubbles grow into macroscopic cavitation bubbles. Since pressure in liquids is related to velocity, at the regions where velocity is high enough so that the static pressure at that particular location becomes less than the vapour pressure, cavitation takes place.

Cavitation erosion is caused by the extremely high pressure peaks that occur during the implosion of cavitation bubbles in the vicinity of seat wall [5-7]. The location of cavitation damage is dependent upon a variety of factors, including valve geometry and flow conditions at injectors.

In solenoid valves cavitation bubbles formed especially over the surface of valve seat region cause material damage when these bubbles rupture (See Figure 2). However, cavitating flow is also desired in solenoid valves due to the requirement of constant mass flow over the ball. Therefore, it is desired to understand its physics and to predict its erosive behaviour.

CFD modelling of cavitation requires two phase modelling due to generation of bubbles in diesel fluid flow within the solenoid valve geometry. Dirke, et al. [8] described the cavitating flow with a two fluid model where liquid and vapour phase are treated separately. For each phase, a transport equation for the averaged volume fraction is used. It is reported that cavitation develops at the narrowest section of the valve seat. Delale et al. [9] presented mathematical theory and numerical simulation of bubbly cavitating unsteady quasi-one-dimensional nozzle flows.

Cavitation models are divided into the Lagrangian (discrete bubble) and Eulerian (continuum) approaches according to their computational framework [2, 10] The Lagrangian approach focuses on the behavior of discrete bubbles using bubble tracking and bubble dynamics equations [11]. The Eulerian approach is based on an approximation of a homogeneous mixture flow. The mixture flow moves at the same velocity, and each phase is identified by solving a volume fraction transport equation. The Eulerian approach was divided into the barotropic relation model [12-14] and two phase mixture flow model [15-18]. The barotropic relation model solves a single continuity equation with a barotropic relation equation between the pressure and density. On the other hand, the two-phase mixture flow model deals with two-phase continuity equations by employing a volume fraction

transport equation. Unfortunately, the volume fraction contains no specific information on the shape or size of the cavitation entities in a volume cell [8]. However, the challenge is to detect the location of bubble collapse zones and their material damage. For non-isothermal simulation walls are defined as adiabatic. Inlet and outlet temperatures are varied.

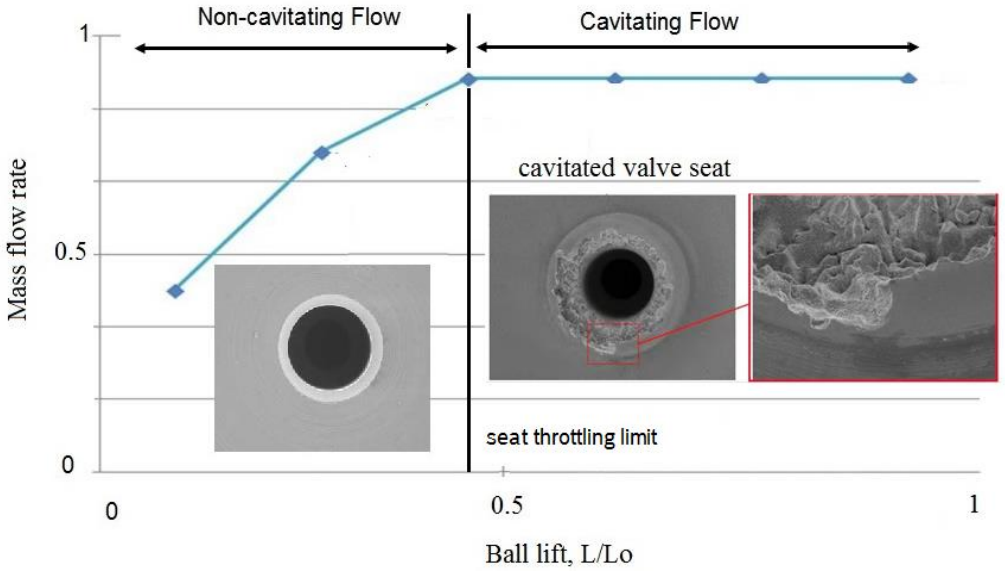

Figure 2. Cavitated valve seat picture shown on the plot of ball lift versus mass flow rate for solenoid valve.

Kayakol [18, 19] presented steady state and transient flow characteristics of bubbly diesel fluid flow in a ball type solenoid valves. It is shown that stagnation effect due to deceleration of flow in front of the ball, detachment and re-attachment of flow along surface walls can be considered as key points in cavitation analysis due to their influence on bubble formation.

Cavitation erosion results from successive bubble collapse generating very high local pressures and temperatures. When the pressure loads exceed the elastic limit of the material, the material undergoes permanent deformations leaving microscopic pits. When the bubbles collapse very near material surface, microjets impact the surface. The initial incubation period of the material response to the erosion cavitation flow field does not involve any mass loss. With repeated impacts, hardening of the material surface layer develops, the deformation of the material accumulates, and finally micro-failures occur resulting in material removal and thus weight loss. A review of physical mechanisms and erosion models is available elsewhere [20].

Commercial CFD codes provide a cavitation model but not a cavitation erosion model which deals with material damage of bubble collapse. Main parameters of conventional cavitation models, namely pressure and vapour volume fractions, indicate where bubbles are generated but do not explain how cavitation damage on material surfaces. Therefore, a cavitation erosion model needs to be used together with a cavitation model for the assessment of erosion.

In the present study, the cavitation erosion model, MDPR (Mean Depth Penetration Rate) is used as the quantification of the erosive potential of collapsing vapour structures. The cavitation erosion model runs at CFD post-processing stage using a script file. The erosion model of Franc [21] is based on physical analysis of the work hardening process due to successive bubble collapses. Turbulence effect on MDPR is included using turbulent kinetic energy. Thermal effects on cavitation are taken into consideration by solving energy equation, momentum equations and cavitation model. Physical properties (density, specific heat and viscosity) are used as a function of temperature. Time dependent cavitation efficiency is defined using valve seat throttling limit which is a threshold ball lift for reaching cavitating regime.

2. Cavitation model

The homogeneous mixture modelling approach is used for numerical simulation of cavitating flow in solenoid valve injectors. The diesel liquid and vapour phases are assumed to be in thermal equilibrium and treated as interpenetrating continua. Diesel can either evaporate or condensate according to pressure difference between liquid and vapour phases. Surface tension, fluctuations of bubbles, viscous effects and interphase velocity slip are neglected.

Compressible formulation for liquid phase and incompressible formulation for vapour phase is applied. The density, ρ_l and viscosity, μ_l of diesel liquid are defined as a function of pressure, P and temperature, T. Constant density, ρ_v and viscosity, μ_v are defined for vapour phase. The density, ρ and viscosity, μ of the mixture is scaled with vapour volume fraction, α;

$$\rho = \alpha\rho_v + (1-\alpha)\rho_l(P,T) \quad (1)$$

$$\mu = \alpha\mu_v + (1-\alpha)\mu_l(P,T) \quad (2)$$

The subscripts v and l refer to vapour and liquid respectively.

The Reynolds-averaged continuity and momentum equations for the mixture flow are as follows:

$$\frac{\partial\rho}{\partial t} + \frac{\partial(\rho u_j)}{\partial x_j} = 0 \quad (3)$$

$$\frac{\partial(\rho u_i)}{\partial t} + \frac{\partial(\rho u_i u_j)}{\partial x_j} = \frac{\partial P}{\partial x_i} + \frac{\partial}{\partial x_j}\cdot\left[(\mu+\mu_t)+\left(\frac{\partial u_i}{\partial x_j}+\frac{\partial u_j}{\partial x_i}-\frac{2}{3}\frac{\partial u_k}{\partial x_k}\delta_{ij}\right)\right] \quad (4)$$

where u_i is the velocity in the i-direction, μ and μ_t are laminar and turbulent viscosities, respectively. Turbulent flow is modelled with Shear-Stress-Transport which solves both the velocity and length scale from two separate transport equations.

The set of Eqns. (3) and (4) are solved with the equations of cavitation model. A cavitation process is governed by the transport equation of vapour volume fraction, α as follows:

$$\frac{\partial(\rho_v\alpha_v)}{\partial t} + \frac{\partial(\rho_v\alpha_v u_j)}{\partial x_j} = \dot{m} \quad (5)$$

where $\dot{m}$ is the source term that represents evaporation and condensation during phase transition.

The calculation of source term for the vapour volume fraction equation is based on Rayleigh-Plesset (RP) Equation (RP). The first order approximation of RP equation is given as follows [6]:

$$\frac{dR}{dt} = \sqrt{\frac{2}{3}\frac{(P_v - P)}{\rho_f}} \quad (6)$$

where R denotes the radius of the spherical bubble. The total interphase mass transfer rate per unit volume, $\dot{m}$ is:

$$\dot{m} = N_B\frac{dm_B}{dt} = N_B\rho_v\frac{d}{dt}\left(\frac{4}{3}\pi R^3\right) = N_B\rho_v 4\pi R^2\frac{dR}{dt} = \frac{3\alpha\rho_v}{R}\sqrt{\frac{2}{3}\frac{(P_v-P)}{\rho_l}} \quad (7)$$

where N_B is the number of bubbles per unit volume, which is calculated from vapour volume fraction, α

$$\alpha = V_B N_B = \frac{4}{3}\pi R^3 N_B \quad (8)$$

The rate of vaporization and condensation is controlled by liquid–vapour pressure differences ($P_v - P$). The Eqn. (7) can be generalized as

$$\dot{m} = F\frac{3\alpha\rho_v}{R}\sqrt{\frac{2}{3}\frac{(P_v-P)}{\rho_l}}\,\mathrm{sgn}(P_v - P) \quad (9)$$

where F is an empirical factor. When the local pressure is lower than the vapour pressure, vapour forms. The vaporization and condensation processes have different time scales. When the local

pressure is higher than the vapour pressure, any vapour present in the fluid will condense at a relatively slow rate. The coefficient F is equal to F_v=50 and F_c=0.001 for vaporization and condensation, respectively. As the vapour volume fraction increases, the nucleation site density must decrease accordingly, because there is less liquid. For vaporization, volume fraction, α in Eqn. (7) is replaced with $\alpha_{nuc}(1-\alpha)$. The value of α_{nuc} which is the empirically determined volume fraction of the nucleation sites, is equal to 5.0e^{-4}.

2.1 Cavitation Erosion model

Cavitation erosion results from successive bubble collapse generating very high local pressures and temperatures. When the pressure loads exceed the elastic limit of the material, the material undergoes permanent deformations leaving microscopic pits. The initial incubation period of the material response to the erosion cavitation flow field does not involve any mass loss. With repeated impacts, hardening of the material surface layer develops, the deformation of the material accumulates, and finally micro-failures occur resulting in material removal and thus weight loss.

In the present study, the quantification of the erosive potential of collapsing vapour structures is based on the analytical model of Franc [21, 22]. The method includes both the knowledge of material deformation and flow aggressiveness.

The erosion damage depends primarily on the mean amplitude $\bar{\sigma}$ the impact loads relative to σ_Y and σ_U. Three cases can happen:

(i) Elastic case ($\bar{\sigma} < \sigma_Y$): The impacts are supposed to cause no damage at all. Pressure pulses whose amplitude is lower than the yield strength are supposed to cause no damage and the material is supposed to return to its original state after unloading. A way of increasing cavitation erosion resistance is enhancing the elastic limit of the material.

(ii) Plastic case ($\sigma_Y < \bar{\sigma} < \sigma_U$): Successive impacts cause first the progressive hardening of the material without any mass loss and then its rupture, and the penetration of the damage after the work-hardening process is completed. Work hardening is also known as strain hardening. The relationship between stress (σ) and amount of strain (ε) is described by a power law as follows;

$$\sigma = \sigma_Y + K\,\varepsilon^n \tag{10}$$

where K is the constant and n is the exponent of stress-strain relationship.

At the beginning of cavitation attack, the virgin material is very ductile and able to absorb a large part of impact energy by plastic deformation. Total energy absorbed by the material, W is the area below the stress/strain curve is defined as follow:

$$W(\varepsilon_1) = \int_{x=0}^{l}\left[\int_{x=0}^{\varepsilon(x)} \varepsilon\, d\varepsilon\right]\bar{S}dx = \varepsilon_1\bar{S}L\left(\frac{\varepsilon_1}{\varepsilon_u}\right)^{\frac{1}{\theta}}\frac{\sigma_Y+\beta K\varepsilon_1^n}{1+\theta} \tag{11}$$

where surface strain ε_1 is corresponding to impact load $\bar{\sigma}$ and

$$\beta = \frac{1+\theta}{(1+n)(1+\theta+n\theta)} \tag{12}$$

(iii) Erosion case ($\bar{\sigma} > \sigma_U$): The material is ready to rupture at its surface. No mass loss is expected until surface strain reaches the ultimate strain ε_U corresponding to the ultimate tensile strength σ_U. Mass loss appears after exposure to cavitation. When ε_U increases up to ε′ where L increases up to ΔL+ L This is expressed as

$$\Delta L = L\left[\frac{\varepsilon'}{\varepsilon_u}\right]^{\frac{1}{\theta}} - 1 \tag{13}$$

where ΔL is the thickness eroded during the time of τ i.e., the time necessary for the surface to be fully covered exactly once by the cavitation impacts. L is the thickness of the hardened layer for complete hardening.

The mean depth of penetration rate (MDPR) which is the volume loss rate per unit surface area is defined as

$$MDPR = \frac{\Delta L}{\tau} = \frac{L}{\tau}\left[\frac{\varepsilon'}{\varepsilon_u}\right]^{\frac{1}{\theta}} - 1 \tag{14}$$

As can be seen from Eqn. (14) the steady-state erosion rate MDPR is proportional to L/τ. The thickness L of the hardened layers is a feature of the material, whereas the covering time τ is a feature of the fluid flow. The term in bracket is a multiplicative factor, which depends primarily on flow aggressiveness. The covering time τ is defined as

$$\tau = \frac{1}{N\bar{S}} \tag{15}$$

where N is impact rate and $\bar{S}$ is the mean size of impact area. The rate N, which is also called as bubble collapse intensity is defined from bubble number density, $\dot{n}$ as follows

$$\dot{n} = \frac{3\left(\frac{\partial \alpha}{\partial t}\right)}{4\pi R_{\max}^3} \tag{16}$$

$$N = \frac{3\left(\frac{\partial \alpha}{\partial t}\right)}{4\pi R_{\max}^3} = \left(\frac{3}{4\pi R_{\max}}\right)\left[\frac{3F_c\alpha}{R_{\max}}\sqrt{\frac{2}{3}\frac{|P_v - P|}{\rho}}\right] sign(P_v - P) \tag{17}$$

The incubation time t_{inc} is defined as

$$t_{inc} = \frac{1}{N\bar{S}}\left[\frac{W(\varepsilon_U)}{W(\varepsilon_1)}\right] \tag{18}$$

where $W(\varepsilon_U)$ and $W(\varepsilon_1)$ are absorbed energy due to strain ε_U and ε_1, respectively.

The MDPR given in Eqn. (14) can be re-expressed as

$$MDPR = \frac{\Delta L}{\tau} = N\bar{S}L\left[\frac{\bar{\sigma} - \sigma_Y}{\sigma_U - \sigma_Y}\right]^{\frac{1}{n\theta}} - 1 \tag{19}$$

The Eqn. (19) is obtained by using Eqn. (10) which is written for $\bar{\varepsilon}$ instead of ε' as

$$\Delta L = L\left[\frac{\bar{\varepsilon}}{\varepsilon_u}\right]^{\frac{1}{\theta}} - 1 = L\left(\frac{\bar{\sigma} - \sigma_Y}{\sigma_U - \sigma_Y}\right) \tag{20}$$

In the model main parameters related to material side are yield strength (σ_Y), ultimate strength (σ_U), and thickness of hardened layer (L). On the fluid side, the erosive potential of cavitating flow or flow aggressiveness is described in terms of the mean amplitude, rate and mean size area of the hydrodynamic impact loads.

In this study MDPR is used as a cavitation index and implemented as a post processing tool. The script file is run with CFX post-processer. The definition of MDPR given in Eqn. (19) is redefined as a volumetric quantity

$$MDPR \approx N(0.2R_{\max})^2 L \tag{21}$$

where L =200 μm and R_{max}= 10 μm. The term given in bracket at Eqn. (19) is taken as one. Because the value of $\bar{\sigma}$ is smaller than the material yield strength for the case under consideration.

The impact pressure P on a rigid wall can be given from classic water hammer formula as [6]

$$P = \rho c v \tag{22}$$

where v is the velocity of bubble jet (or perpendicular component of impact velocity), ρ is the density and c is pressure wave velocity (which is equal to the speed of sound, 1500 m/s for water). The mean amplitude of impact loads $\bar{\sigma}$ can be expressed as follows

$$\bar{\sigma} = \rho\, c \max\left[(-\frac{\partial R_B}{\partial t}),0\right] \tag{23}$$

where velocity is represented by time derivative of bubble radius R or the rates of growth of bubbles R_B. Details of the RP equation can be found elsewhere [8-10].

The material damage on the surface exposed to cavitating flow is caused by high velocity liquid jet impact to the solid surface. A microjet velocity may not be calculated from the RP Equation which assumes spherical symmetry, Eqn. (6). The microjet velocity is given as [23]

$$v_{jet} = 8.97\gamma^2\sqrt{\frac{p - p_v}{\rho}} \tag{24}$$

where γ is the non-dimensional distance of the bubble centre from the surface. The critical velocity v_{Crit} which forms a pit is defined as [23]

$$v_{Crit} = \sqrt{\frac{p_y}{\rho_l}\left(1-\left(1+\frac{p_y}{B}\right)^{1/n}\right)} \tag{25}$$

where P_y= 300MPa and n=7.

2.2 Solenoid valve

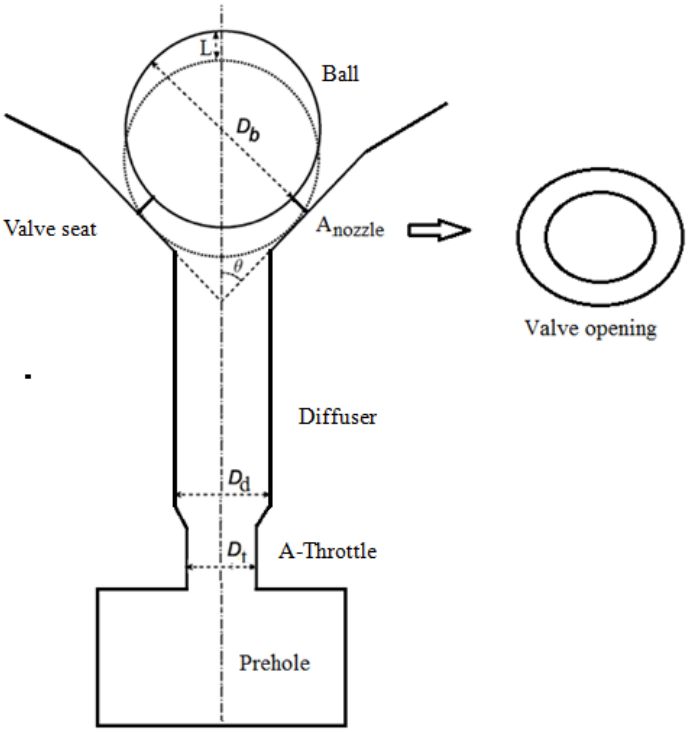

Figure 3. Flow area of valve opening

Figure 3 shows the flow area of valve opening which is defined by ball lift for ball type solenoid valve. The gap between ball and seat is called as seat nozzle. The flow area of nozzle as a function of ball lift L_b is calculated from [24]

$$A_{nozzle}(L_b) = \frac{\pi}{2} L_b \sin\theta\,(x\sin\theta + D_b) \tag{26}$$

where D_b is ball diameter, θ half chamfer angle. When the ball is moving up the seat nozzle area increases with higher ball lifts and exceeds the area of flow restriction which is a-throttle shown in Figure 3. The minimum ball lift for seat throttling limit, L_{stl_min} is found by equating flow area of nozzle to area of flow restriction in a-throttle as follows

$$L_{stl\_min} = \frac{\pi D_t^2}{4} \Big/ \frac{\pi}{2} \sin\theta \, (x \sin\theta + D_b) \tag{27}$$

where D_t is a-throttle diameter. In the range of ball lift [$L_b - L_{stl\_min}$] the flow area is bounded by the seat nozzle area. Therefore, non-cavitating flow regime occurs in a-throttle. When L_b is greater than L_{stl_min} throttling effect starts and cavitating flow in a-throttle exists.

As can be seen from Figure 3 a diffuser is attached to a-throttle. The maximum ball lift seat throttling limit, L_{stl_max} is found by equating flow area of seat nozzle to flow area of diffuser as follows

$$L_{stl\_max} = \frac{\pi D_d^2}{4} \Big/ \frac{\pi}{2} \sin\theta \, (x \sin\theta + D_b) \tag{28}$$

where D_d is diffuser diameter. In the range of ball lift [$L_{stl\_min} - L_{stl\_max}$] the flow area is bounded by a-throttle. The cavitating flow in a-throttle still exists. The seat throttling limit which shows constant mass flow rate over the ball can be reached at the ball lift of $L_{b\_throttling}$, which is $L_{stl\_min} < L_{stl} < L_{stl\_max}$. The value of $L_{b\_throttling}$ can be found from 3D transient analysis. If $L_b > L_{stl\_max}$ the presence of ball does not affect cavitation in seat region.

2.3 Time dependent cavitating efficiency

It is conventional the use of cavitation number, C_a, to characterize how close the pressure in the liquid flow is to the vapour pressure It is defined as

$$C_a = \frac{P - P_v}{1/2 \rho v^2} \tag{30}$$

Cavitation number which shows the severity of cavitation is not suitable for solenoid valve injectors due to moving component, namely, ball which changes pressure and velocity in the system with the lift position.

A new cavitation indicator showing transient nature of solenoid valve is required. Time dependent cavitation efficiency, η_{cav}, for a solenoid valve is defined using the time requirements for maximum and minimum seat throttling limits. In cavitating flow condition mass flow rate becomes constant when uniform pressure occurs in a prehole attached before a-throttle. However, it takes time to get almost uniform pressure in prehole due to valve opening and closing during fuel injections. The injection time t_{cav_inj} is defined as

$$t_{cav\_inj} = t_{stl\_min} + t_{stl} \tag{31}$$

where t_{stl_min} is the corresponds to $L_b < L_{stl\_min}$. t_{stl} is the time required to reach seat throttling limit which corresponds to $L_{stl\_min} < L_{stl} < L_{stl\_max}$. t_{cav_inj} is the injection time at constant mass flow under cavitating flow condition. The cavitating efficiency of injection time is defined as

$$\eta_{cav} = \frac{t_{stl} - t_{stl\_min}}{t_{stl} + t_{stl\_min}} \tag{31}$$

The cavitating efficiency can be increased if the time of seat throttling, tstl is decreased at a lower ball lift. One of the solutions could be a uniform pressure in the prehole before flow restriction unit. Because, uniform pressure is not desired to keep mass flow rate constant over the ball valve (see Figure 9). Another solution may be lowering prehole pressure in a short period of time so that cavitating flow condition can be reached at lower ball lifts.

2.4 Numerical setup

The liquid fluid and vapour properties are is defined as “compressible Diesel” and the vapour, respectively. The flow is considered at isothermal conditions. Because of the rotational symmetry of

the valve, a quasi two-dimensional grid (one layer sector) is used. The grid and the geometry are generated with the ICEM-HEXA grid generation software. Both 2D and 3D geometries of solenoid valve are generated. 4.5 million Mesh is used for 3D geometry. The numerical settings for the cavitation model are set to default values. "Maximum Density Ratio" is set to 32000. The 2D and 3D calculations are performed by solving the Reynolds-averaged Navier-Stokes equation using the CFD solver CFX [25, 26].

2.5 Boundary conditions

Inlet and opening boundary condition type is applied for inlet and outlet, respectively. At the boundaries of the domain pressure boundary conditions are applied. The back pressure is one bar and the inlet pressure is varied. The flow is considered at isothermal conditions with a constant temperature of 40°C. Inlet and outlet temperatures are defined at the inlet and outlet with corresponding static pressure values.

3. Results and discussions

The numerical prediction of cavitating flows is a difficult problem due to density ratio between liquid and vapour which bring a lot of difficulties for the convergence. It is necessary to use very fine grid size to get rid of convergence problem. Effect of mesh size on cavitation erosion index MDPR is taken into account. Three different mesh sizes which are named as basecase, fine and finer mesh cases are considered. CFX runs with xeon64 of Intel processor. Grid dependency on cavitation erosion index, MDPR is shown on Table 1 which also gives number of nodes versus CPU values for a 2D geometry. The MDPR is a scalar variable. It is calculated for each cell. The comparison of cases in terms of MDPR is done for a point defined in valve seat region. As node size increases CPU usage increases. The use of finer mesh slightly changes the value of MDPR. The node number of 19646, is good enough for using cavitation–erosion index, MDPR.

Table 1. Grid dependency on cavitation erosion index, MDPR [18].

	Nodes	CPU, min	MDPR $x10^{-10}(m^3/s)$
Basecase	19646	12	1.84
Fine mesh	105302	62	1.86
Finer mesh	133946	74	1.87

3.1 Effect of flow variables on cavitation

The difficulty in CFD analysis of cavitating flow in a solenoid valve comes from the fact that the locations of bubble formation does not mean where bubbles implode. This is because bubbles form at low pressures but collapse at high pressure regions, especially below the ball and near valve seat. Figure 4 indicates the variation of scaled pressure along Line 1 (close to wall of valve seat), Line 2 (close to wall of a-throttle), Line 3 (along centre) and Line 4 (below ball). Pressure is reduced as the fluid passes through the minimum flow area (a-throttle) where there exists highest velocity. Cavitation occurs near walls of a-throttle due to local pressure drop below the vapour pressure of the diesel fuel. This cause vapour bubbles to form. Pressure recovery in the diffuser is very poor due to narrow and micron size diffuser geometry. Therefore, amount of bubble collapse within diffuser is very low compared to that for valve seat region where bubbles rapidly collapse below the ball. As can be also seen from Line 4 of Figure 4 high local pressures are generated below the ball due to stagnation effect of ball, which is explained in detail elsewhere [19].

The flow pattern in valve geometry can be considered as high speed fuel jet flow which occurs after throttling of high pressure fuel. Figure 5 gives the plot of Mach number a long Line 1 (close to wall of valve seat), Line 2 (close to wall of a-throttle) and Line 5 (close to wall of diffuser). The Mach number is below one, the flow velocity is lower than the speed of sound and flow is subsonic.

The CFD results show the flow variables decisively affect cavitation. These are (a) the velocity of the fluid medium, (b) the pressure occurring in the fluid medium, (c) the proportion of vapour to

total volume of fluid medium (vapour volume fraction) and (d) temperature. Figure 6 shows the variation of scaled velocity, vapour volume fraction, temperature and pressure versus distance in diffuser along Line 5. The line is chosen such that the variation of flow variables can be seen along wall of diffuser which acts as a bubble generator. Although bubbles first form along walls of flow restriction unit, a-throttle, as a thin sheet cavitation process continues in the next component, diffuser, due to very high velocity fuel jet emerging from a-throttle. The velocity increases in diffuser until it hits the ball. The pressure along the line is below the vapour pressure of liquid diesel, 30 mbar. It is seen on the graph as zero pressure along the line. At the beginning of the line vapour volume fraction is very high due to accumulation of vapour in the corner which is subject to vortex formation. Then, vapour volume fraction along wall of diffuser through valve seat region decreases. It is more likely high vapour content in the corner is convected via fuel jet in the diffuser.

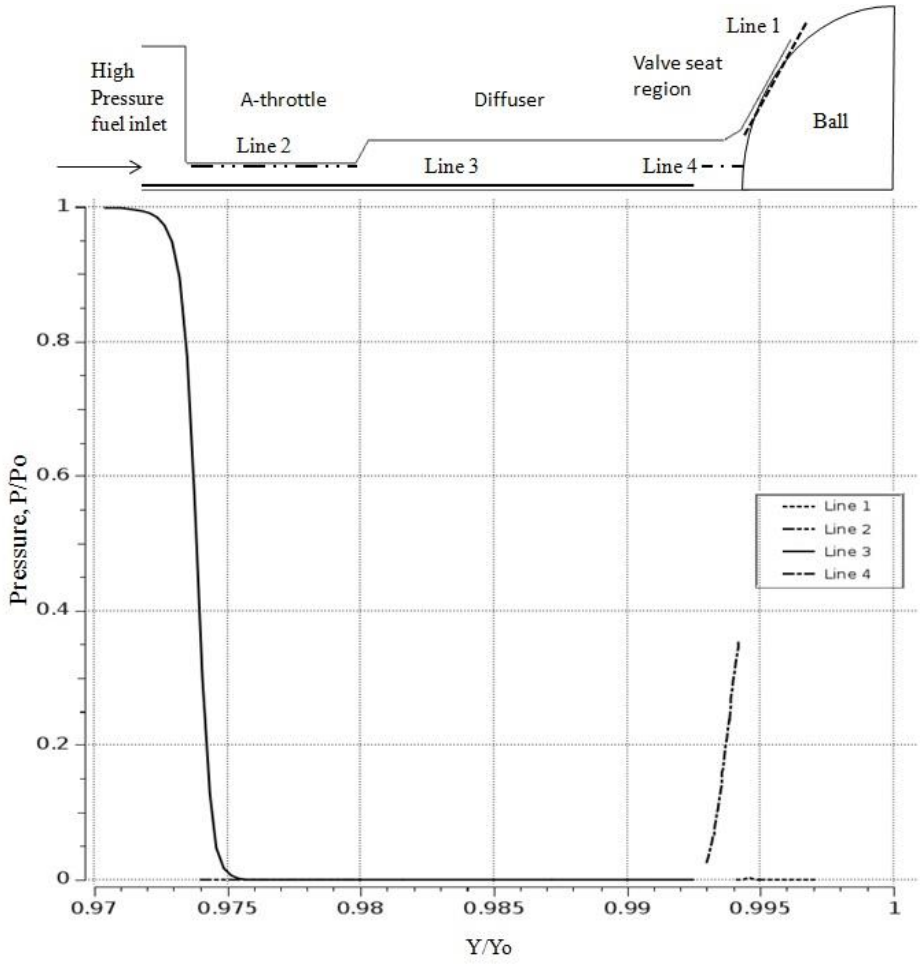

Figure 4. Plot of scaled pressure versus distance along Line 1 (close to wall of valve seat), Line 2 (close to wall of t a-throttle), Line 3 (along centre) and Line 4 (below ball).

High pressure diesel fuel is a compressible fluid. Its temperature increases due to compression during throttling. The temperature profile in the diffuser along the line 5 at Figure 5 is almost uniform. This indicates that vapour content which varies in diffuser is not related to temperature of the medium. Cavitation model has no thermal term for bubble evaporation (see Eqn. (9)). A parametric study is done with different the inlet pressure and temperature of solenoid valve in order to further investigate thermal effect on cavitation. The comparison of measurements and CFD predictions for seat and outlet temperatures are shown in Table 2. Four different cases having different inlet temperature and pressure are taken into account. The temperature and pressure values are scaled with inlet and outlet values. Predictions are in good agreement with the measurements.

Temperatures at the seat and outlet are higher than inlet temperature due to contraction of compressible diesel fuel at the flow restriction unit (a-throttle). As inlet pressure increases the seat and outlet temperature increases. The outlet temperature is a little bit lower than seat temperature due to expansion after seat region in solenoid valve. These results does not differentiate temperature rise in the injector whether it is coming from either throttling or bubble collapse. Therefore, cavitation model needs to be modified for temperature effect for bubble formation.

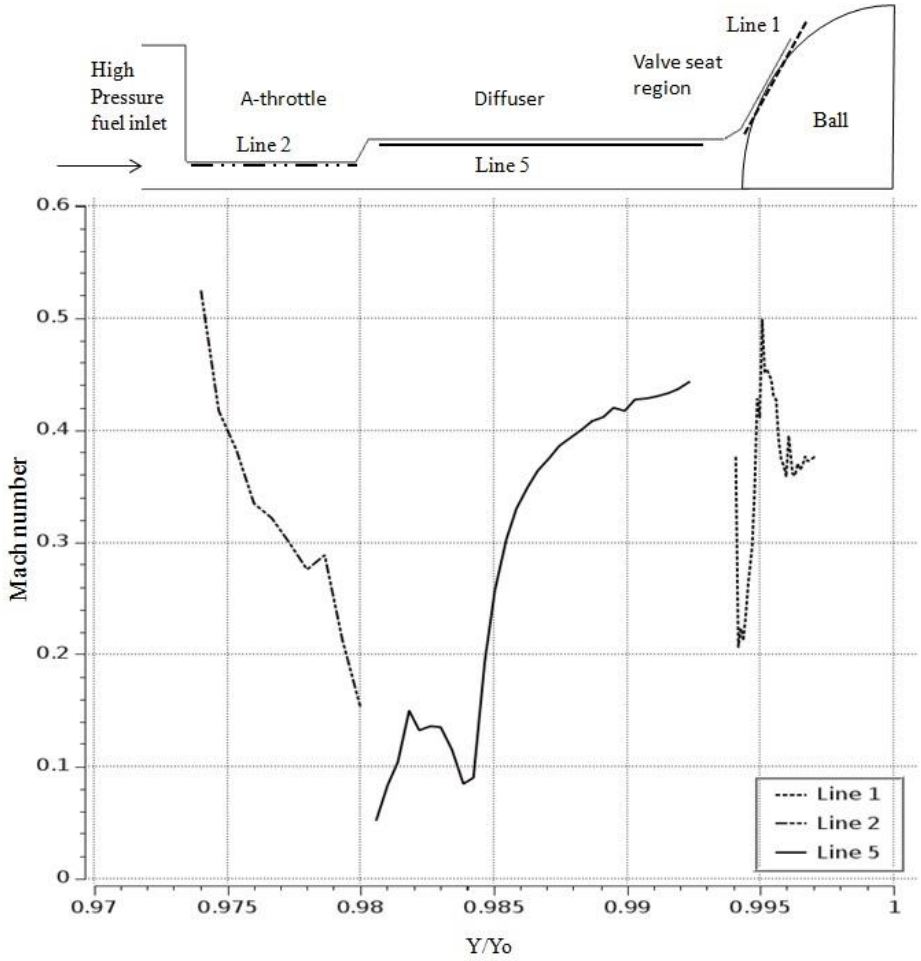

Figure 5. Plot of Mach number a long Line 1 (close to wall of valve seat), Line 2 (close to wall of a-throttle) and Line 5 (close to wall of diffuser).

Table 2. Comparison of scaled measured temperature with predictions at different pressures.

	Case 1		Case 2		Case 3		Case 4	
$\widehat{P}_{inlet}(=P/P_{inlet})$	1.00		0.90		1.00		0.90	
$\widehat{T}_{inlet}(=T/T_{inlet})$	1.00		1.00		0.91		0.91	
	Exp.	Model	Exp.	Model	Exp.	Model	Exp.	Model
$\widehat{T}_{seat}(=T/T_{inlet})$	1.17	1.18	1.13	1.15	1.09	1.11	1.06	1.08
$\widehat{T}_{out}(=T/T_{inlet})$	1.16	1.17	1.12	1.13	1.09	1.06	1.05	1.07

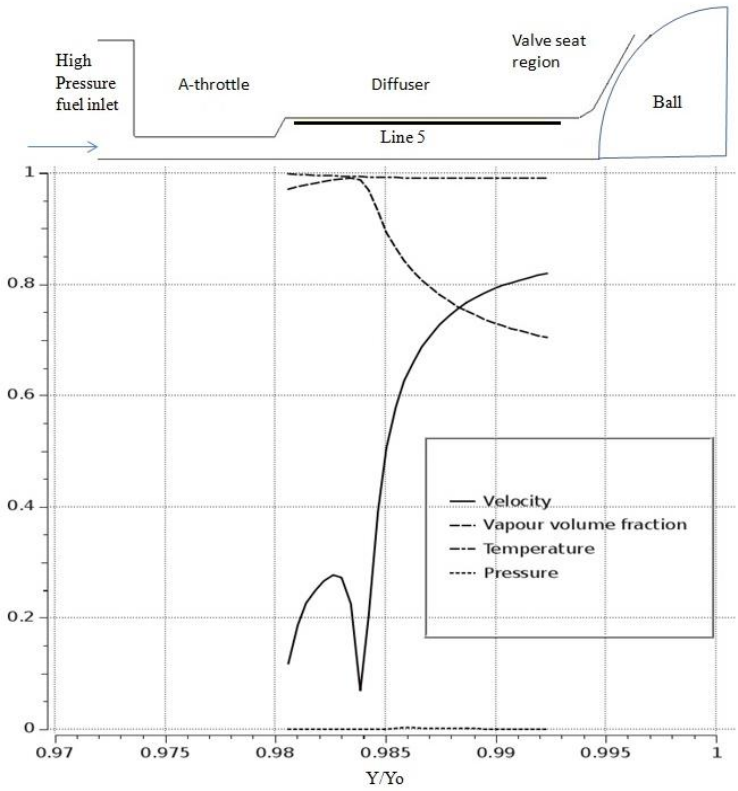

Figure 6. Plot of scaled velocity, vapour volume fraction, temperature and pressure versus distance along Line 5 (close to wall of diffuser).

3.2 Effect of valve seat throttling on cavitation

Time dependent cavitation efficiency, η_{cav}, for a solenoid valve is defined using the time requirements for maximum and minimum seat throttling limits. As can be seen on the Figure 2 seat throttling limit which corresponds to certain level of ball lift is the threshold for the cavitation in the solenoid valve injector. Before seat throttling limit no cavitation occurs. After seat throttling limit high pressure cavitation erosion in the valve seat region takes place. Figure 7 shows the scaled flow area as a function of valve opening defined by ball lift. Flow area is calculated between minimum and maximum ball lifts for seat throttling, L_{stl_min} and L_{stl_max}. If the ball is lifted 28% cavitating flow starts in a-throttle. At the 60% of valve opening seat throttling limit is reached. It means that at 28% of valve opening flow area around the ball is equal to flow area of flow restriction unit, a-throttle. The 15 % of injection time is used for 28% of valve opening.

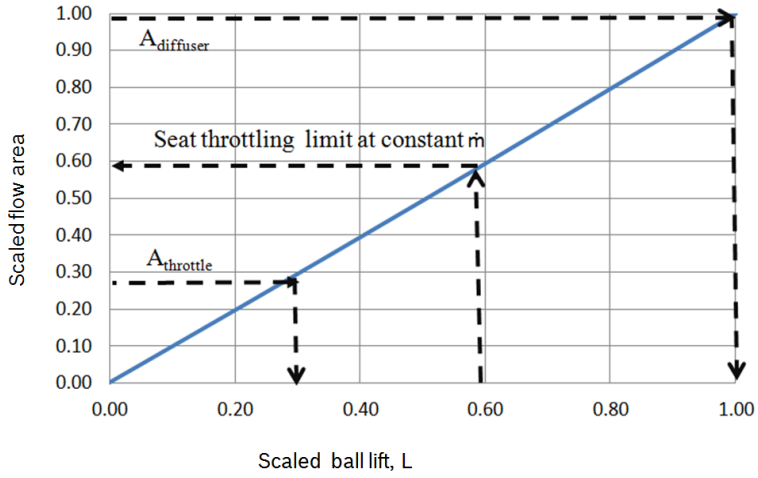

Figure 7. Scaled flow area as a function of valve opening defined by ball lift.

As can be seen from Figure 8 flow is under non-cavitating flow condition. Bubbles are formed neither in a-throttle nor in diffuser. The 30% of extra injection time is required for reaching seat throttling limit which indicates the start of cavitation erosion. Figure 9 indicates the time dependent pressure and mass flow rate before throttling of solenoid valve. T_{stl_min} and T_{stl} is about 15 % and 30% of injection time, respectively. This means that %45 of injection time is required for obtaining cavitating flow condition or reaching seat throttling limit. η_{cav} is equal to 0.33 (=15-30/15+30). If seat throttling can be achieved at lower ball lifts η_{cav} increases and erosion damage on valve seat may decrease. Because cavitation erosion increases at higher ball lifts. This is due to increase in velocity which results in lower pressure in narrow flow passages where bubble forms.

The variation of mass flow rate as a function of ball lift shown in Figure 2 and transient mass flow rate shown in Figure 9 indicate that uniformity of mass flow rate under cavitating flow condition is not almost same. Variations in transient mass flow rate can be observed. The results shown in Figure 2 and Figure 9 are obtained from 2D and 3D studies respectively. The main difference in the simulations of 2D and 3D simulations is the selection of boundary condition of pressure inlet at the prehole of valve geometry. In the 2D simulation uniform pressure inlet is defined. In the 3D simulation a realistic boundary condition is given. The variation of pressure at the prehole inlet is taken into consideration. Such a comparison shows importance of the selection of pressure type boundary condition for cavitation simulations. Variation in pressure directly affects mass flow rate. Uniform pressure inlet defined as a boundary condition produces constant mass flow rate, as shown in Figure 2. If pressure distribution at the inlet is considered variations in mass flow rate can occur, as shown in Figure 10. Variations in mass flow rate can affect cavitation behaviour in the valve. This is not desired because asymmetric valve seat damages can be observed.

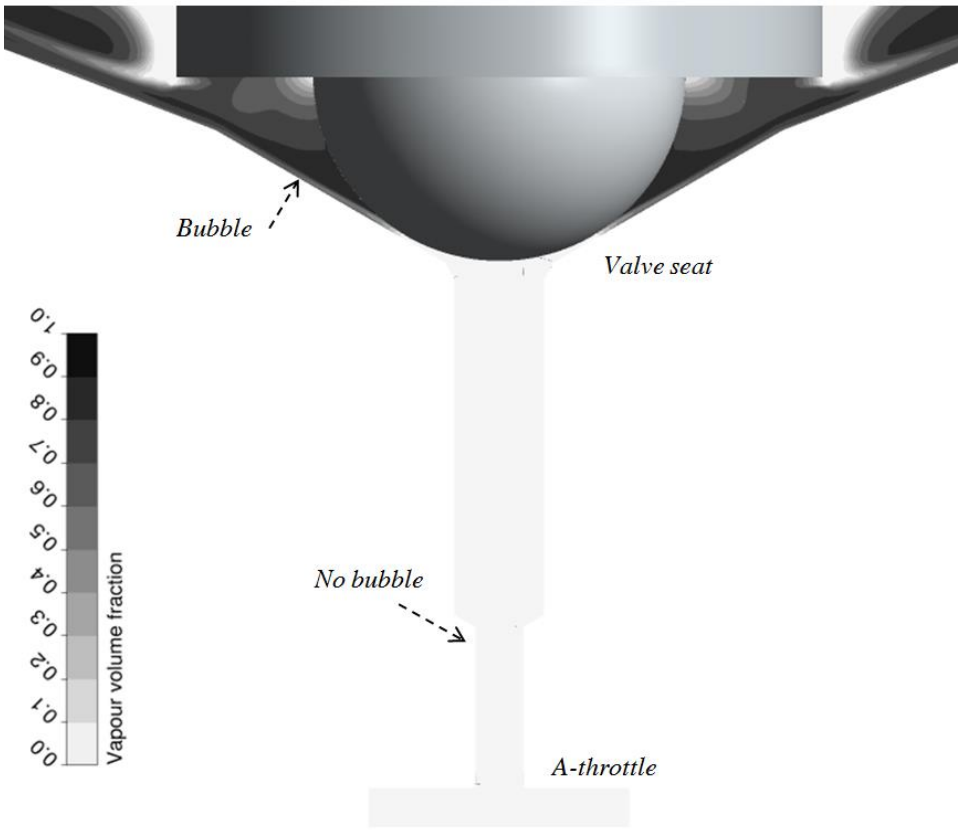

Figure 8. Distribution of vapour volume fraction at ball lift of L_{stl_min} where flow opening at valve seat is equal to flow restriction area at A-throttle.

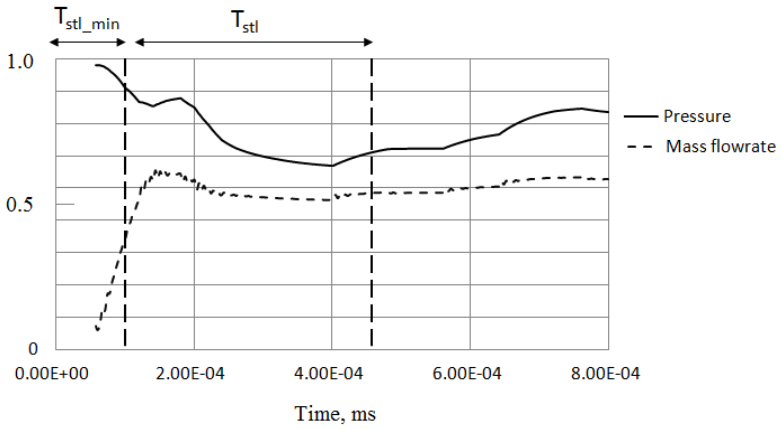

Figure 9. Time dependent pressure and mass flow rate before throttling of solenoid valve.

3.3 Cavitation erosion damage

Bubbles which implode near walls cause material loss especially in valve seat region. Bubbles which implode away from surface below the ball causes ball cavitation. Figure 10.(a) shows the contours of vapor volume fraction at open ball position and pressure impact of bubble implosion over ball in solenoid valve. The scale of the figure on the right is arranged in a way that highest vapor volume fraction has dark colour and lowest one has light colour. Vapour generation in solenoid valve geometry is associated with pressure drops below vapour pressure of diesel. The high vapour fraction in the diffuser is high due to poor pressure recovery. The presence of vapour near to surface can cause high cavitation erosion damage. Vapor volume fraction is very high at the corners of diffuser but there is no cavitation erosion. This is because bubbles form at low pressures but implodes at higher pressures. The scale of the figure on the left is arranged such that highest pressure impact of bubble implosion has dark colour and lowest one has light colour. The pressure impact is only shown on the ball. Bubbles at the centre of diffuser implode and cause high pressure impact over the ball.

One of prediction of cavitation model, namely, condensation of bubbles which is calculated from interphase mass transfer rate from vapour to liquid can be used as a cavitation indicator. Figure 10.(b) shows the contours of interphase mass transfer between liquid and vapor of diesel. The scale of the slide is arranged in a way that the evaporation (vapor generation) has positive (+) values shown with a light color. The condensation has negative (-) values with a dark color.

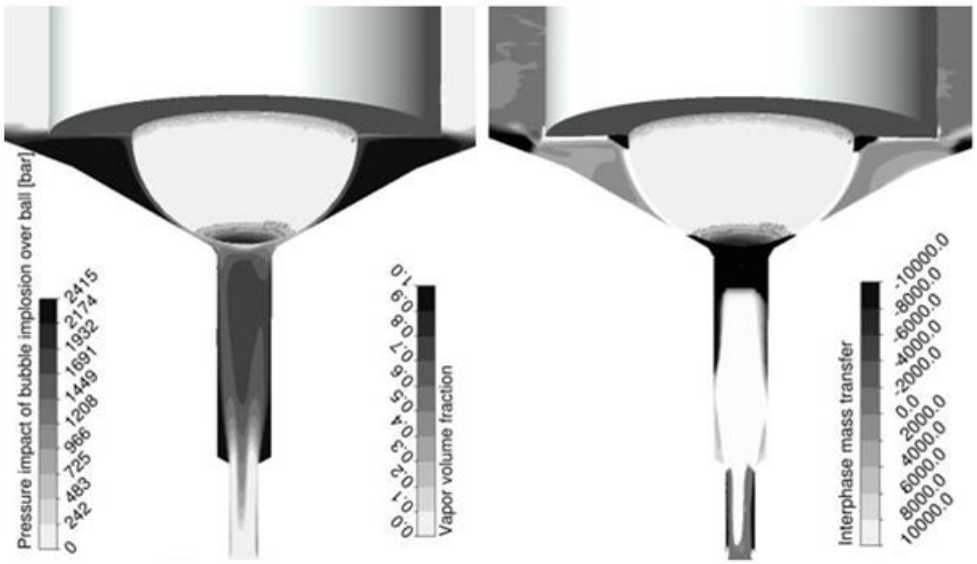

Figure 10. (a) Contours of vapor volume fraction and pressure impact of bubble implosion over ball in solenoid valve and (b) interphase mass transfer between liquid and vapour.

3.4 Cavitation erosion index, MDPR

Since cavitation erosion is the result of the material response to repeated impact loads, it appears fundamental to accurately determine impact loads in order to be able to predict the erosion damage. The mean amplitude of pressure impact defined in Eqn. (21) requires accurate prediction of microjet velocity. Table 3 shows variation of MDPR with cavitation bubble microjet velocities defined in Eqn. (6) and Eqns. (24) and (25). The values of MDPR are given for a point defined in valve seat region. The Eqn. (6) gives the lowest microjet velocity which is bubble interface velocity. The pressure impact to wall is less than material yield strength. This is corresponding to Elastic case ($\bar{\sigma} < \sigma_Y$) in which the impacts are supposed to cause no damage at all. Therefore, the Eqn. (6) can provide misleading results for cavitation erosion. At higher microjet velocities calculated from empirical correlations given in Eqns. (24) and (25) the pressure impact to wall is higher than material yield strength. This means that bubble collapse may cause plastic deformation. The Eqn. (24) gives minimum microjet velocity which can form a pit. Therefore, microjet velocities can be calculated either from Eqn. (24) or Eqn. (25).

A material having high resistance to cavitation erosion is generally shows a long incubation time. As can also be seen from Table 3 as microjet velocity increases incubation time for damage of bubble collapses decreases. Therefore, higher MDPR value or lower incubation time can be considered as an indication of severe cavitation erosion.

Table 3. The cavitation index MDPR at different microjet velocities of a single bubble.

Microjet velocity (m/s)	Pressure impact (Bar)	Incubation time (s)	MDPR (m^3/s)
54 (Eq. 6)	650	2.3e-5	1.84e-10
237 (Eq. 25)	2900	9.0e-5	8.10e-10
713 (Eq. 24)	8700	7.1e-11	2.40e-09

3.5 Effect of model parameters on cavitation erosion

The cavitation model under consideration has four model parameters. As can be seen from Eqn. (9) the interphase mass transfer rate is a linear function of the volume fraction of the nucleation sites, α_{nuc}, vaporization constant, F_v, and the condensation rate constant of F_c. It is inversely proportional to the nucleation site radius, R_{nuc}, Accuracy of the cavitation model is based on the selection of these model constants. Distribution of vapour volume fraction along a-throttle and diffuser as a function of α_{nuc} and F_v are shown in Figure 11. Dark regions show higher vapour volume fractions. The default value of r_{nuc}, and F_v are $5.0e^{-4}$ and 50, respectively. As the value of α_{nuc} and F_v increase the vapour generation increases and more vapour is seen near surfaces. Higher values of either α_{nuc} ($=1.0e^{-2}$) or F_v (=250) produce almost similar distribution of vapour volume fraction in valve geometry in valve geometry.

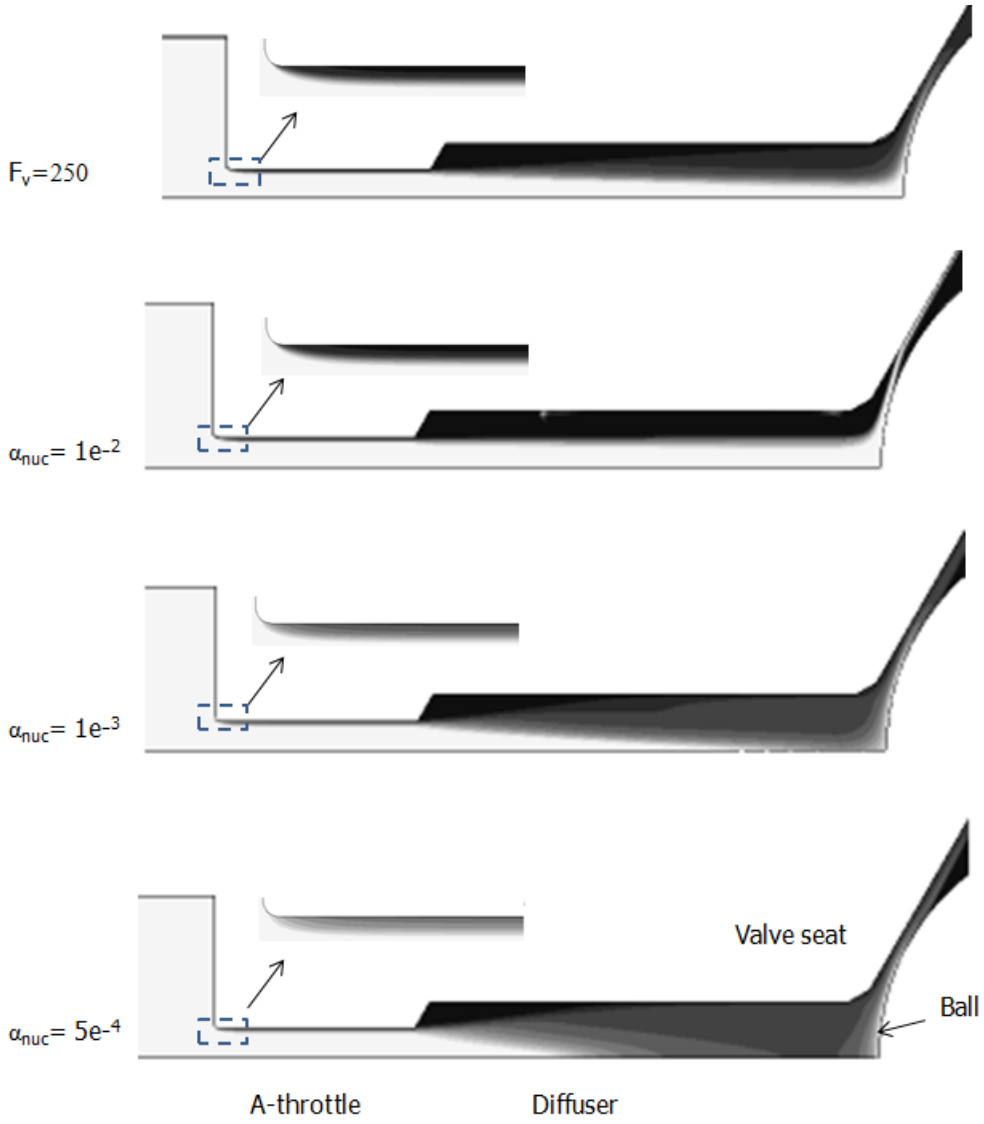

Figure 11. Distribution of vapour volume fraction as a function of α_{nuc}, the volume fraction of the nucleation sites and F_v, vaporization coefficient.

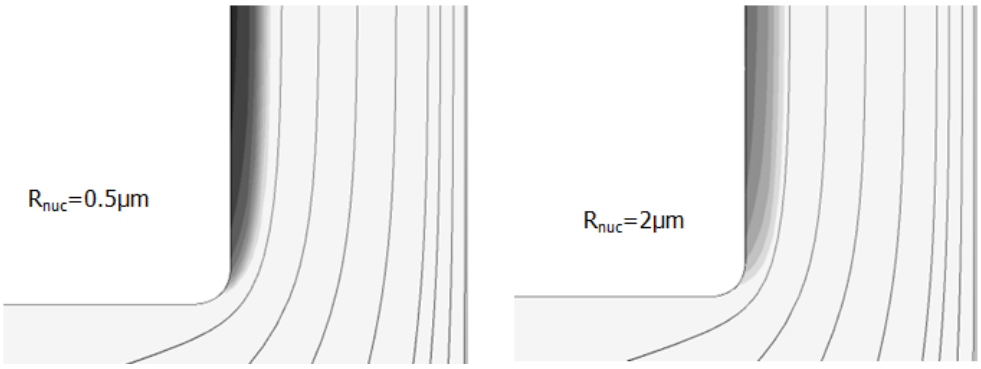

Figure 12. Streamlines and distribution of vapour volume fraction at the entrance of A-throttle.

Figure 12 gives the streamlines and distribution of vapour volume fraction as a function of R_{nuc}, the nucleation site radius at the entrance of a-throttle. As the value of R_{nuc} decreases the vapour generation increases as expected. Table 4 shows the variation of the cavitation index MDPR for

different condensation rate constant of F_c. The values of MDPR are given for a point defined in valve seat region. The default value of F_c is 0.01. Higher values of F_c mean high bubble collapse and more cavitation erosion damage. Therefore, any combination of model parameters can produce different results for vapour formation (bubble generation) and condensation (bubble collapse). These model parameters are also used for estimation of cavitation erosion damage. This means that predictive accuracy of cavitation erosion model is very sensitive to cavitation model parameters.

Table 4. The cavitation index MDPR for different condensation rate constant of F_c.

F_c	MDPR (m^3/s)
0.01 (Default of CFX)	1.84E-12
1 (MDPR script)	1.84E-10
10	1.84E-09

4. Conclusion

Cavitation erosion damage in solenoid valve injectors is investigated with a two phase mixture model suited for bubble-liquid flow. Cavitation is desired for the sake of keeping mass flow rate constant in channel flow. The aim of investigation is not to avoid cavitation but control it so that bubbles may collapse away from valve seat. A standard cavitation analysis done with the distribution of vapour volume fraction and pressure is not good enough. It is shown that a cavitation erosion model which considers bubble dynamics and material properties needs to be used together a cavitation model. The parametric analysis for both cavitation and cavitation erosion models indicates that non-geometrical model parameters hinder alleviation of cavitation erosion damage with geometrical modifications of solenoid valve due to poor pressure recovery in the micro channels of the injector. The optimization of model parameters may require several test results. Therefore, more generalized methodology for cavitation and cavitation erosion models can be a further future study.

One of prediction of cavitation model, namely, condensation of bubbles which is calculated from interphase mass transfer rate from vapour to liquid can be used as a cavitation indicator. More accurate one is the MDPR which considers both the knowledge of material deformation and flow aggressiveness. The predictive accuracy depends on some variables such as microjet velocity, cavitation model parameters and turbulent kinetic energy. The most important one is microjet velocity calculated from the bubble interface velocity which is provided by Rayleigh-Plesset equation. It is much lower than the microjet jet velocity that can cause a pit or plastic deformation on a material surface. Therefore, accurate calculation pressure impact calculated from Rayleigh-Plesset equation can be misleading. The cavitation model parameters like vaporization and condensation constants produce different results for vapour formation (bubble generation) and condensation (bubble collapse). These model parameters are also used for estimation of cavitation erosion damage. This means that predictive accuracy of cavitation erosion model is very sensitive to cavitation model parameters.

Although the effect of temperature on fluid properties is taken into account there is no variation of volume vapour fraction with respect to temperature. It means that without modification of cavitation model the solution of energy equation with momentum equation does not show thermal effect on cavitation.

Conventional cavitation number which considers local pressure drop and fluid velocity does not cover transient nature of valve opening and closing. Time dependent cavitating efficiency, η_{cav}, is defined for solenoid valve due to moving component, namely, ball which changes pressure and velocity in the system with its the lift position. It is related to seat throttling limit which is a threshold ball lift for cavitating flow regime.

NOMENCLATURE

c Speed of sound [m/sec]
C_a Cavitation number
D_b Ball diameter [m]
D_t A-throttle diameter

F_c	Condensation coefficient
F_v	Vaporization coefficient
K	Constant of stress-strain relationship
k	Turbulent Kinetic Energy
L	Thickness of hardened layer [m]
L_b	Ball lift [m]
$\dot{m}$	Source term in the volume fraction equation, [s^{-1}]
n	Exponent of stress-strain relationship
N_B	Number of bubbles per unit volume [m^{-3}]
N	Rate of impact load or bubble collapse intensity [$1/m^2s$]
P	Pressure [bar]
P_v	Vapour saturation pressure [bar]
R	Radius of cavitation bubble [m]
$\overline{S}$	Mean size of impact area [m^2]
t_{inc}	Incubation time [s]
v	Velocity of bubble jet [m/s]
$W(\varepsilon_U)$	Absorbed energy due to strain ε_U [J]
$W(\varepsilon_1)$	Absorbed energy due to strain ε_1 [J]
α	Vapour volume fraction
ΔL	Thickness eroded [m]
ε	Strain [s^{-1}]
ε_1	Strain corresponding to impact load $\overline{\sigma}$ [s^{-1}]
ε'	Rapture strain [s^{-1}]
μ	Dynamic viscosity [Pa.s]
η_{cav}	Cavitating efficiency
$\overline{\sigma}$	Mean amplitude of pressure impact [Pa]
σ_Y	Yield strength [Pa]
σ_U	Ultimate tensile strength [Pa]
ρ	Density [$kg \cdot m^{-3}$]
Θ	Shape factor of the strain profile
θ	Half chamfer angle [rad]
τ	Covering time [s]

Subscripts

ini	Initial
inj	Injection
B	Bubble
crit	Critical conditions
i, j	Cartesian tensor indices
nuc	Nucleation site
stl	Seat throttling limit
t	Turbulent
l	Liquid
v	Vapour

Abbreviations

MDPR	Mean Depth of Penetration Rate [m^3/s]
RP	Rayleigh-Plesset
TKE	Turbulent Kinetic Energy

5. References

[1] Leonhard R, Pauer T, Rückle M. Schnell M. Solenoid common rail injector for 1800 bar, MTZ Motortechnische Zeitschrift, 71: 10-15, 2010.

[2] Beierer P. Experimental and numerical analysis of hhydraulic circuit of a high pressure common rail diesel fuel injection system, PhD, Tampere University of Technology, Tampere, Finland, 2007.
[3] Ferrari A, Mittica A, Spessa E. Benefits of hydraulic layout over driving system in piezo-injectors and proposal of a new-concept CR injector with an integrated Minirail, Applied Energy ; 103: 243-255. 2013
[4] Seyken XLJ. Modelling of common rail fuel injection system and Influence of fluid properties on injection process, Proceedings of VAFSEP; Dublin, Ireland, 2004.
[5] Brennen CE. Cavitation and bubble dynamics. Oxford, UK: Oxford University Press; 1995.
[6] Brennen CE. Fundamentals of multiphase flow. New York, USA: Cambridge University Press; 2005.
[7] Martynov S. Numerical simulation of the cavitation process in diesel fuel injectors, PhD, University of Brighton, UK, 2005.
[8] Dirke, M. Simulation of cavitating flows in diesel injectors, Oil & Gas Science and Technology, 54: 223-226, 1999.
[9] Delale CF. Pasinlioglu S., Baskaya, Z. Mathematical theory and numerical simulation of bubbly cavitating nozzle flows, Berlin, Germany: Springer-Verlag; 2012.
[10] Marjollet LB. Specialist committee on cavitation, Proceedings of 25th ITTC, Vol. 3. Fukuoka, Japan, 1-61, 2008.
[11] Chahine GL. Nuclei effects on cavitation inception and noise. In: 25th Symposium on naval hydrodynamic, St. John's, Newfoundland and Labrador, Canada, 2004.
[12] Delannoy Y, Kueny JL. Two phase flow approach in unsteady cavitation modeling. ASME cavitation and multiphase flow forum, Toronto, Canada, 1990.
[13] Kubota A, Kato H, Yamaguchi H. A new modelling of cavitating flows: a numerical study of unsteady cavitation on a hydrofoil section. J Fluid Mech; 240:59–96, 1992.
[14] Chen Y, Heister SD. A numerical treatment for attached cavitation. J Fluids Eng; 190: 299–307, 1994.
[15] Schnerr G, Sauer J. Physical and numerical modeling of unsteady cavitation dynamics. In: 4th International conference on multiphase flows, New Orleans, LA, US: 2001.
[16] Singhal AK, Athavale MM, Li H, Jiang Y. Mathematical basis and validation of the full cavitation model. J Fluids Eng; 124: 617–24, 2002.
[17] Senocak I, Shyy W. A pressure-based method for turbulent cavitating flow computations. J Comput Phys; 176: 363–83, 2002.
[18] Kayakol N. CFD modelling on flow characteristics of two phase flow in solenoid valves, Int. Symp. on Convective Heat and Mass Transfer, CONV-14, Turkey: 2014.
[19] Kayakol N. CFD modeling of cavitation in solenoid valve for diesel fuel injection, 8th International Conference on Computational and Experimental Methods in Multiphase and Complex Flow, Spain: 2015.
[20] Terwisga TJC. A review of physical mechanisms and erosion risk models, Proceedings of the 7th International Symposium on Cavitation CAV2009–, 17-22, 2009.
[21] Franc, J. Incubation Time and Cavitation Erosion Rate of Work-Hardening Materials, J. Fluids Eng, 131:1-14, 2009.
[22] Kim K, Chahine G, Franc J, Karimi A, Advanced experimental and numerical techniques for cavitation erosion prediction, Dordrecht , Netherlands, Springer; 2015.
[23] Dular, M and Coutier-Delgosha, O, Numerical modelling of cavitation erosion, Proceedings of FEDSM2008, 2008 ASME Fluids Engineering Conference, August 10-14, Jacksonville, Florida USA, 2008.
[24] Viel, A, Strong Coupling of Modelica System-Level Models with Detailed CFD Models for Transient Simulation of Hydraulic Components in their Surrounding Environment, 8th International Modelica Conference - Dresden, Germany - 20-22 March, 2011.
[25] ANSYS CFX 15.0 Theory manual, ANSYS, Inc., 2014.
[26] Bakir F, Rey R, Gerber AG, Belamri T, Hutchinson B. Numerical and experimental investigations of the cavitating behaviour of an inducer, International Journal of Rotating Machinery, 10:15-25, 2004.